Shunted Josephson Junctions and Optimization of Niobium Integrated Matching Circuits

Mariia S. Shevchenko, Artemiy A. Atepalikhin, Fedor V. Khan, Lyudmila V. Filippenko, Artem M. Chekushkin, and Valery P. Koshelets, *Member, IEEE*

***Abstract*—Josephson junctions (JJs) with non-hysteretic I-V characteristic and high critical parameters are required for many applications; in particular, they are needed to create tunable THz range oscillators. We fabricated and studied shunted superconductor-insulator-superconductor (SIS) Nb-AlO_x-Nb tunnel junctions with an area of about 1μm^2, estimated their parameters, and compared them with theoretical models. To assess the performance of shunted junctions in the terahertz range, their characteristics were studied under the influence of a high-frequency signal; the estimated value of the characteristic voltage for the shunted junction at a high frequency is about 1 mV. To improve the circuit parameters, a new type of the shunting based on application of NIS junctions was proposed, which reduces the influence of parasitic inductance, expands the frequency range of the generator, and decreases the size of the structure. The JJs with a new type of shunting have been fabricated and studied. The niobium integrated circuits intended for matching the superconducting oscillator and an SIS junction as a microwave detector were designed, fabricated, and tested. Such structures are required for studying the spectral characteristics and analyzing the operation of the oscillator. The developed circuits have demonstrated efficient operation at frequencies from 300 to 700 GHz; the experimental results are in good agreement with the simulated characteristics. The results obtained will be implemented for further development of the THz range oscillators.**

***Index Terms*—Josephson effect, superconducting integrated circuits, superconducting devices, thin film circuits.**

Manuscript received September 29, 2021; revised October 29, 2021; accepted November 1, 2021. Date of publication November 23, 2021; date of current version December 22, 2021. This work was supported by the Russian Science Foundation under Project 20-42-04415. The equipment of USU 352529 "Cryointegral" was used to carry out the research; USU is supported by a grant from the Ministry of Science and Higher Education of the Russian Federation, under Agreement 075-15-2021-667. *(Coresponding author: Mariia S. Shevchenko.)*

Mariia S. Shevchenko is with the Kotel'nikov Institute of Radio Engineering and Electronics RAS, 125009 Moscow, Russia, and also with the Moscow Institute of Physics and Technology (National Research University), 125009 Moscow, Russia (e-mail: shevchenko@hitech.cplire.ru).

Artemiy A. Atepalikhin and Fedor V. Khan are with the Kotel'nikov Institute of Radio Engineering and Electronics RAS, 125009 Moscow, Russia, also with the Institute for Physics of Microstructures RAS, 603950 Nizhny Novgorod, Russia, and also with the Institute for Physics of Microstructures RAS, 603950 Nizhny Novgorod, Russia (e-mail: atepalikhin@hitech.cplire.ru).

Lyudmila V. Filippenko and Artem M. Chekushkin are with the Kotel'nikov Institute of Radio Engineering and Electronics RAS, 125009 Moscow, Russia.

Valery P. Koshelets is with the Kotel'nikov Institute of Radio Engineering and Electronics RAS, 125009 Moscow, Russia, and also with the Institute for Physics of Microstructures RAS, 603950 Nizhny Novgorod, Russia.

Color versions of one or more figures in this article are available at https://doi.org/10.1109/TASC.2021.3130103.

Digital Object Identifier 10.1109/TASC.2021.3130103

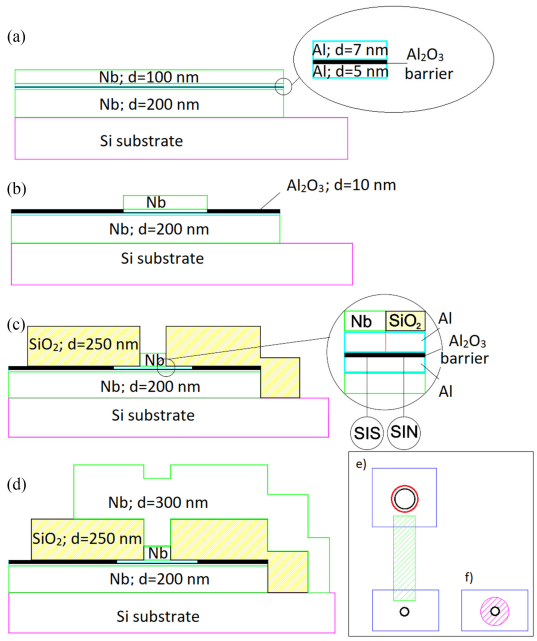

Fig. 1. The technological process for fabrication of a JJ with NIS-shunting: (a) Deposition of a four-layer structure Nb-AlO_x/Al-Nb. (b) Formation of a "large" junction by reacting ion etching and anodization of the upper layer of aluminum outside the "large" junction. (c) Formation of a "small" SIS junction, deposition of an insulator layer. (d) Deposition of the upper (counter) electrode; topologies of shunted junctions presented on the same scale (counter electrode is not shown). (e) Shunting using a thin-film resistor and (f) proposed new version of shunting by integrated NIS junction.

I. Introduction

TO CREATE tunnel junctions with non-hysteretic current-voltage characteristics and high critical parameters external shunts are required [1]–[5]. Traditionally, a shunt is realized by thin metallic stripe and, therefore, has rather big inductance, which constraints the operation of such devices at high frequencies [3]. In addition, direct contact of the shunt to the base electrode is required. As a result, the area occupied by shunted junction considerably exceed area of the initial superconductor-insulator-superconductor (SIS) junctions. As a solution for all these problems, a new topology of shunt formed by a normal metal-insulator-superconductor (NIS) junction surrounding the SIS junction is suggested. The process of fabricating a topology with NIS shunting is presented in Fig. 1. At the first stage of the study, we evaluated parameters of the traditionally shunted SIS junction and verified them by

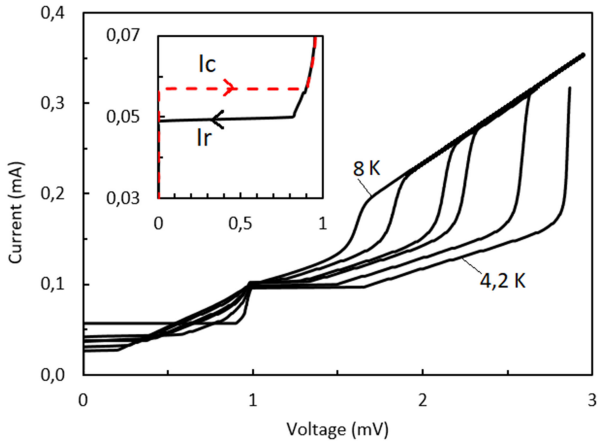

Fig. 2. The IVCs of the shunted junction at different temperatures, measured with increasing current. The insert shows the part of the IVC for one temperatures at increasing and decreasing of the bias current; the arrows indicate the direction of the current. Also, the method of determination the value of the critical current (I_c) and the return current (I_r) is shown.

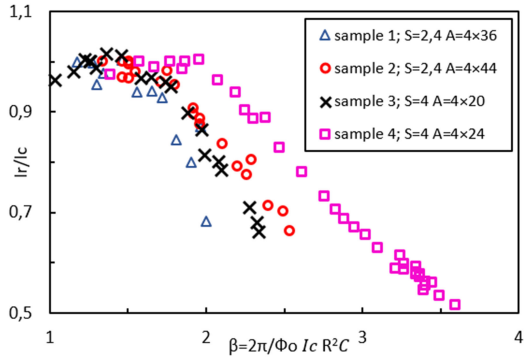

Fig. 3. Hysteresis parameter Ir/Ic vs the junction capacitance parameter βc for the various samples of shunted Josephson junctions for different temperatures (4.2-10K). The samples differ in the junction area (S in μm2) and the degree of shunting. A is the shunt dimension in μm (width$\times$ length) of the resistor film. The parameters of samples 1–4 are provided in Table I.

TABLE I
PARAMETERS OF THE SHUNTED JUNCTIONS

	Sample 1	Sample 2	Sample 3	Sample 4
S, μm^2 –junction area	1.4	1.4	2.8	2.8
A, shunt dimension in μm	4×36	4×44	4×20	4×24)
A, "squares"	9	11	5	4
Rtotal, Ω	7.7	8.8	4.5	5.3
Vc, μV	440	485	536	692
β_c(T=4.2 K)	2	2.5	2.3	3.6

The parameters of the four shunted junctions, the characteristics of which are shown in Fig. 3. The table presents the areas, the shunt dimension, as well as the total resistance (normal junction resistance and shunt resistance), the characteristic voltage and the parameter βc.

theoretical models [6]–[8]; see Section II. These data were compared with preliminary results for the Josephson junction (JJ) with NIS shunting (Sections III and IV).

To compare properties of the junctions with different type of shunting at high frequency, the shunted junctions were integrated with flux-flow oscillator (FFO) fabricated on the same chip [9], [10]. Frequency of the FFO can be tuned electronically from 300 to 700 GHz by changing magnetic field produced by integrated control line. Details of the design and experimental test of the matching circuits between FFO and JJ are presented in Sections V and VI.

II. JUNCTIONS, SHUNTED BY THIN-FILM RESISTOR

A. Hysteresis Characteristics

To determine the main hysteresis characteristics, the IV curve (IVC) measurements of shunted Nb-AlO_x-Nb structures were carried out in the temperature range of 4.2-10 K (Fig. 2). The IVC feature observed at voltages near 1 mV could be explained by a geometric resonance in the electrodes of the structure, created by currents of Josephson generation. Position of these resonances should be properly taken into account at designing generators, based on arrays of shunted JJs. The presence of this feature on the IVC indicates the existence of a powerful generation in the structure at frequencies of the order of 500 GHz (a characteristic voltage of the order of 1 mV), which can be delivered to a microstrip line.

The values of the critical currents (I_c) and the return currents (I_r) were determined from the experimental data (see the insert in Fig. 2). The dependences of their ratio on the parameter $\beta_c = 2\pi/\Phi_0 I_c R^2 C$ [3], [7], [11], [12] for four different samples are presented in Fig. 3. The parameters of samples 1–4 are provided in Table I. The experimental data obtained lie between the theoretical curves, calculated for the RSJN model (nonlinear resistive model) with $R_j/R_n = 2$ and for the RSM model (resistively shunted model) [7], [12]. The R_j is the resistance of the junction at voltages $V<2\Delta/e$ (Δ is energy gap), and R_n is normal junction resistance.

B. High-Frequency Characteristics.

To assess the performance of shunted junctions in sub-terahertz range, their characteristics were studied under the influence of a high-frequency signal generated by on-chip FFO, operating in the frequency range 300-700 GHz. Measurements were carried out using conventional matching circuits [9]. More details concerning matching structures will be presented in Sections V and VI. Under the influence of a high-frequency signal on the junction, a series of vertical steps appears at the voltages $V_n = n\hbar\omega/2e$ ($\hbar$ is Planck's constant, and e is the electron charge), called Shapiro steps. They appear due to the synchronization of Josephson generation by an external signal [7].

Fig. 4(a) shows the IVCs of the shunted junction at different signal power at a frequency of 500 GHz; the power was varied to obtain the dependences of the amplitude of the 1st and 2nd Shapiro steps on the amplitude of the high-frequency signal [7], [13] and to estimate the V_c value from high-frequency measurements. The amplitude of the step with the number n, on condition that the frequency of the external periodic signal

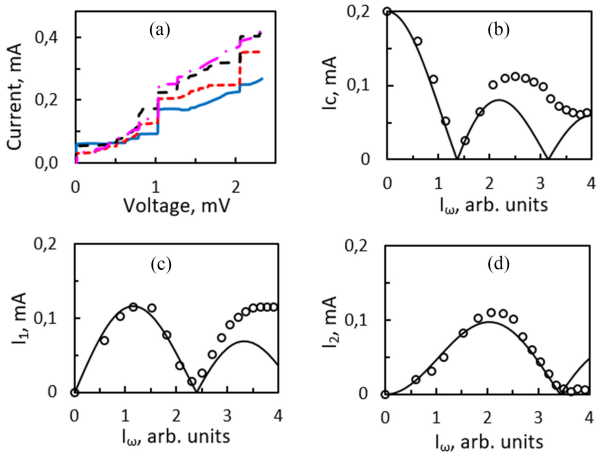

Fig. 4. (a) The I-V curves of junctions with thin-film resistor at different signal power, provided by on-chip FFO at a frequency of 500 GHz. Double amplitude of the critical current I_c(b), the first I_1 (c) and the second I_2 (d) Shapiro steps in mA vs the amplitude of the high-frequency signal I_ω (arb. units) at a frequency of 500 GHz. Experimental data are presented by points, the dependences for the resistive junction model at low dumping are shown by solid lines.

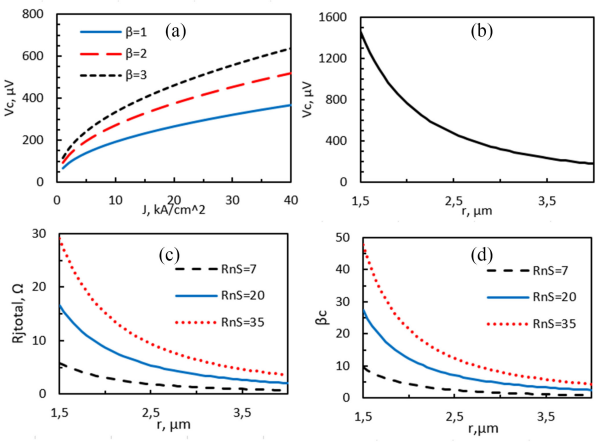

Fig. 5. (a) Calculated critical voltage depending on the current density for different values of the parameter β_c for junction with thin-film resistor. (b) Calculated critical voltage depending on the outer radius of NIS shunt. Calculated total resistance under the gap (c) and parameter β_c depending on the outer radius of NIS shunt for different R_nS values in $\Omega*\mu m^2$. Area of the SIS junction is 1.4 μm^2.

$f = \omega/2\pi$ is less than or equal to the characteristic frequency $\omega_c = 2eV_c/\hbar$, is given by the formula $I_{n\pm} = I_c\, J_n\, (I_\omega/I_c)$ [7], [13]. The value J_n is the Bessel function of the first kind of order n and I_ω is the amplitude of the external signal.

The amplitude of the first steps was measured for different frequencies and for junctions with different areas, depending on the generator power, which varied due to changes in the FFO current at a constant voltage (frequency) [9]. The dependences of the doubled I_c and the amplitude of the first and second current steps on the amplitude of the signal current I_ω at a frequency of 500 GHz are shown in Fig. 4(b), (c), (d). The value of the I_ω in the first approximation is proportional to the square root of value of the FFO superconducting current [10] at a voltage of 1 mV.

Good agreement of the oscillations with the unmodified Bessel function at a frequency of 500 GHz allows us to conclude that the characteristic voltage of the shunted junction at high frequencies $V_c{}^{RF}$ is about 1 mV. As predicted in [7], junctions with a lower V_c value perform worse at high frequencies; the agreement of the oscillations with the Bessel functions was observed when exposed at frequencies below 360 GHz.

III. Estimation of Shunted Junction Parameters

In order to determine the geometric characteristics of the junctions and current density, which are necessary to get the desired critical parameters, the calculations were carried out. Fig. 4(a) refers to shunting with a thin-film resistor; it is needed to determine what current density is required to create junctions with fixed critical voltage and β_c. Calculations show that the characteristics of such junctions begin to deteriorate at frequencies above 500 GHz due to the influence of the inductance [3] of the thin-film resistor. A new junction topology with NIS-shunting has been proposed to improve the high-frequency properties. To calculate the main parameters we estimated the resistance of the NIS junction under the gap at voltages of about 1 mV by using the analytical expression of current-voltage characteristic of the NIS junction [14]. It was obtained that the resistance under the gap, which is a shunt for the new topology, is 5 times greater than $R_n{}^{NIS}$. Fig. 5(b), (c), (d) refer to new NIS-shunting and present how calculated parameters depend on the outer radius of this shunt.

Calculation shows, that by increasing the current density (by decreasing R_nS), it is possible to create junctions without hysteresis at V of about 1 mV and with high V_c. For example, for the critical current density 18 kA/cm^2 ($R_nS = 7\ \Omega*\mu m^2$), radius of SIS junction 0.67 μm ($S = 1.4\ \mu m^2$) and outer radius of a NIS junction, $r = 2\ \mu$m, V_c will be approximately 500 μV, while β_c, calculated for measured at dc parameters, will be about 2.5.

IV. Junctions With NIS-Shunting

Junctions with new type of NIS shunting were designed and fabricated; preliminary measurements demonstrated that such shunting topology works as it was expected. The figures below demonstrate IVCs of such junctions for various FFO frequencies (Fig. 6) and for different powers at the FFO frequency of 410 GHz. Fig. 7(a). For a new type of shunting, the dependences of the amplitudes of the steps on the value of the high-frequency signal were also obtained, Fig. 7(b), (c), (d). The experimentally measured amplitudes of the first and second Shapiro steps are as large as doubled I_c value and considerably exceed the theoretical estimations [7], [13]. It means that the amplitude of the Josephson currents at high frequencies is actually larger than expected from I_c measured at dc IVC. The experimental results showed that junctions with such shunting operate well at a frequency of 410 GHz; in order to increase the operating frequency, samples with a higher current density will be fabricated in the future.

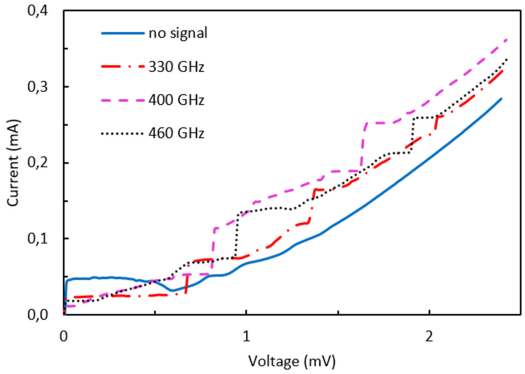

Fig. 6. I-V curves of the junctions with a new type of NIS-shunting without the influence of a signal and under the influence of signals with frequencies of 330, 400, and 460 GHz. Shapiro steps corresponding to the frequencies are observed.

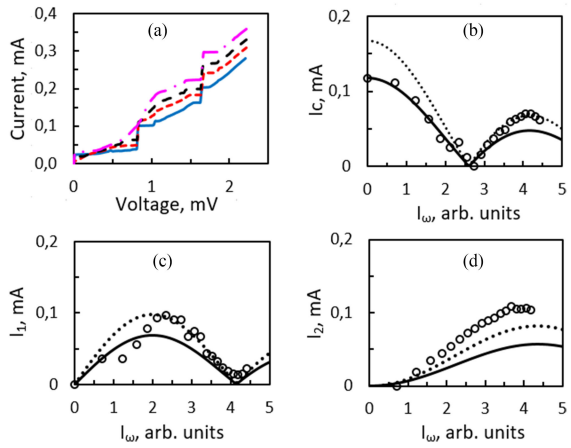

Fig. 7. (a) The I-V curves of NIS-shunted junction at different signal power, provided by on-chip FFO at a frequency of 410 GHz. Double amplitude of the critical current I_c (b), the first I_1 (c) and the second I_2 (d) Shapiro steps vs the amplitude of the high-frequency signal I_ω (arb. units) at a frequency of 410 GHz. Experimental data are presented by points; the dependences for the resistive junction model at low dumping, bound to experiment at $I_\omega = 0$, are shown by solid lines; the same dependences bound to experiment at $I_\omega = 4$ are presented by dash lines.

V. Integrated Coupling Circuits

To study the high-frequency properties of SIS junctions, an on-chip source of electromagnetic radiation and a line for transmitting of this signal are necessary. The already proven long JJ, so-called flux-flow oscillator (FFO), was used as a sub-terahertz generator. It is important to ensure equally good signal transmission in the entire frequency range at which the junction is being studied; that is, the impedance matching coefficient of the FFO and the SIS junctions is high enough for all frequencies. The transmission of the radiated by the FFO signal is carried out through a specially designed integrated matching structure, the parameters of which affect the behavior of the matching coefficient depending on the frequency. A photo of one of these matching circuits is presented in Fig. 8. The geometric dimensions of the elements, as well as the characteristics of the materials used for their manufacture, determine the nature of the signal transmission from the generator to the sample under study.

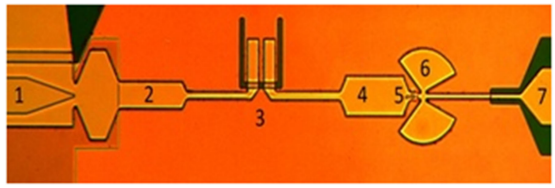

Fig. 8. Photo of the integrated circuit: 1 – Flux-Flow Oscillator; 2- three-stage impedance transformer; 3 - DC block; 4 – two-stage impedance transformer; 5- SIS junction detector with inductive section to compensate the capacitance of the SIS junction in the operating frequency range; 6- radial sectors for high-frequency grounding; and 7- output coplanar line.

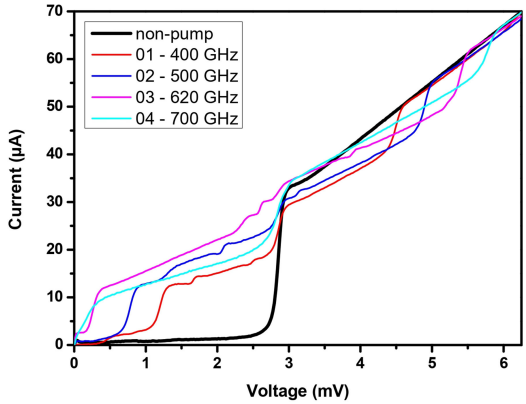

Fig. 9. The I-V curves of the SIS detector: no signal – autonomous IVC of the Nb–AlOx–Nb detector without high-frequency signal; curves 1, 2, 3 and 4 were measured for the FFO operating at 400, 500, 620, and 700 GHz, correspondingly; the critical current of detector is suppressed.

To determine the power that has reached the SIS junction, its pump current is measured under the influence of a high-frequency signal, see Fig. 9. The difference of the currents between the pumped by RF signal and autonomous curves measured at the operating point below the gap, gives the value of the pump current I_{pump}. It is possible to estimate the detected power, knowing its dependence on the current [15] – usually it's about a few tenths of microwatts.

VI. Calculation Models and Their Application

To optimize the parameters of the integrated circuit, two mathematical models were developed to calculate the dependence of the matching coefficient on the frequency for the transmission line. In the first case, the impedance matching coefficient between different parts of the circuit, from the source to the detector (Impedance Matching), is calculated sequentially, in the second method, the transmission matrices of the circuit elements (ABCD matrices) are compiled [16], and the ratio of the power incident at the SIS junction to the power radiated by the generator - Transferred Power Ratio (TPR) is calculated [17]. At frequencies above 0.7 THz, where the energy of the radiation quantum becomes comparable and may even exceed the value of the superconducting niobium gap, the signal from the generator is strongly absorbed in the superconducting electrodes of the transmission line. To account for these losses, the TPR calculation includes a modified Mattis-Bardin theory [18], modified

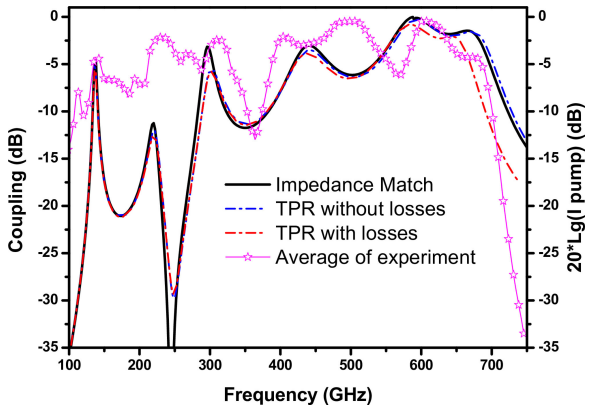

Fig. 10. Calculated coupling coefficient (left axis) between the generator and the mixer for two theoretical models: Impedance Match and transferred power ratio (TPR). Dependence of the pump current on the frequency for the experimental circuit with parameters that were used for the calculation (right axis).

by taking into account the strong coupling effects, which lead to appearance of the intragap states for quasiparticle excitations for the Nb used in the work (as well as for the NbN and NbTiN, which will be used for fabrication of devices with operating frequencies up to 1 THz). These results are shown by the TPR curve with losses in Fig. 10, where three theoretical curves, calculated for the identical set of parameters, are compared with each other and with the experimental results for the circuit with same parameters.

In fact, at the experiment we measure the pump current I_{pump} caused by the FFO power delivered to the of the SIS detector at different FFO frequencies. According to [15] I_{pump} is proportional to $\alpha = eV_{RF}/hf$ at moderate α ($1 < \alpha < 2$); here V_{RF} is high frequency voltage induced by the FFO power; the corresponding RF power is proportional to I^2_{pump}. To compare the experimental result with model calculations (presented in dB) the value $10*\mathrm{Lg}(I^2_{pump}) = 20*\mathrm{Lg}(I_{pump})$ is computed and plotted in Fig. 10. It can be noted that the frequency peaks are in good agreement both between the two calculations and between both calculations and experiment. The TPR model enables us to take into account losses in transmission lines, which become significant at frequencies above the gap (700 GHz for Niobium) and are relatively strong in case of electrodes made of normal metal.

The experimentally observed pumping at low frequencies is due to the generation of the FFO at harmonics of Josephson frequency. It was demonstrated that the pumping observed at voltages of about 0.4–0.7 mV (which corresponds to frequencies of 200–350 GHz) is a "replica" of the pump at frequencies of 400–700 GHz compressed in half along the frequency axis. Even lower along the frequency axis, one can see the pumping caused by the generation of the third harmonic. Note that level of the emitted by FFO power is affected by abrupt transition from Fiske to flux-flow regime at 470 GHz for Nb-AlO_x-Nb junction which corresponds to voltage $V_g/3$ [19].

VII. Conclusion

We fabricated SIS junctions shunted by a thin-film resistor, measured their parameters and hysteresis characteristics; studied their behavior under the influence of a high-frequency signal provided by on-chip FFO. The characteristic voltage of the shunted junctions at high frequencies was measured to be about 1 mV. To minimize cell dimension and decrease inductance of traditional shunts a new type of shunting based on application of NIS junction was proposed and preliminary tested. Advantages of the NIS shunted junctions can be realized for high current density circuits. Two mathematical models of the matching circuit were built; by using these models new versions of the integrated circuits for the frequencies 250–700 GHz were developed. The experimental results for developed circuits agree well with calculations; new designs will be implemented for further improvement and investigations of the THz range oscillators.

References

[1] T. A. Fulton, "Externally shunted Josephson junctions," *Phys. Rev. B*, vol. 7, no. 3, 1973, Art. no. 1189.

[2] H. J. Hartfuss, K. H. Gundlach, and V. V. Schmidt, "Nonhysteretic Josephson tunnel junctions for microwave detection," *J. Appl. Phys.*, vol. 52, no. 9, pp. 5411–5413, 1981.

[3] C. B. Whan and C. J. Lobb "Effect of inductance in externally shunted Josephson tunnel junctions," *J. Appl. Phys.*, vol. 77, no. 1, pp. 382–389, 1995.

[4] E. A. Kostyurina *et al.*, "High-symmetry DC SQUID based on the Nb/ALO*x*/Nb Josephson junctions for nondestructive evaluation," *J. Commun. Technol. Electron.*, vol. 62**,** no. 11, pp. 1306–1310, 2017.

[5] T. Liang *et al.*, "Fabrication and characterization of molybdenum thin-film resistor for superconducting quantum devices," *IEEE Trans. Appl. Supercond.*, vol. 30, no. 7, Oct. 2020, Art. no. 7500304.

[6] A. B. Zorin, K. K. Likharev, and S. I. Turovets, "Dynamics of Josephson tunnel junctions with a finite-width riedel peak," *IEEE Trans. Magn.*, vol. MAG-19, no. 3, pp. 629–632, May 1983.

[7] K. K. Likharev, *Dynamics of Josephson Junctions and Circuits* Philadelphia, PA, USA: Gordon and Breach Science, 1986.

[8] K. K. Likharev, "Superconducting weak links," *Rev. Mod. Phys.*, vol. 51, no. 1, 1979, Art. no. 101.

[9] P. N. Dmitriev, L. V. Filippenko, and V. P. Koshelets, "Applications in superconducting SIS mixers and oscillators: Toward integrated receivers," in *Josephson Junctions. History, Devices, Appl.*, Jenny Stanford, 2017, ch. 7, pp. 185–244.

[10] D. R. Gulevich, V. P. Koshelets, and F. V. Kusmartsev, "Josephson flux-flow oscillator: The microscopic tunneling approach," *Phys. Rev. B***,** vol. 96, no. 2, 2017, Art. no. 024515.

[11] S. K. Tolpygo *et al.*, "Properties of unshunted and resistively shunted Nb/AlO_x-Al/Nb Josephson junctions with critical current densities from 0.1 to 1 mA/μm^2," *IEEE Trans. Appl. Supercond.*, vol. 27, no. 4, Jun. 2017, Art. no. 1100815.

[12] Y. M. Shukrinov, I. R. Rahmonov, and G. Filatrella, "Dependence of the maximal superconducting current on the resonance frequency in a shunted Josephson junction," *J. Exp. Theor. Phys.*, vol. 125, no. 5, pp. 781–788, 2017.

[13] Y. M. Shukrinov *et al.*, "Effects of LC shunting on the shapiro steps features of Josephson junction," *EPL (Europhysics Lett.)*, vol. 110**,** no. 4, 2015, Art. no. 47001.

[14] D. Chouvaev, *Normal Metal Hot-Electron Microbolometer With Superconducting Andreev Mirrors*. Gothenburg, Sweden: Chalmers Univ. of Technology, 2001.

[15] J. R. Tucker and M. J. Feldman, "Quantum detection at millimeter wavelengths," *Rev. Modern Phys.*, vol. 57, no. 4, pp. 1055–1113, 1985.

[16] V. F. Fusco, *Microwave Circuits: Analysis and Computer-Aided Design*. Hoboken, NJ, USA: Prentice Hall, 1987.

[17] D. A. Frickey, "Calculation of S parameters from ABCD parameters with complex normalizing impedances," *Microw. Opt. Technol. Lett.*, vol. 5, no. 12, pp. 613–615, 1992.

[18] D. C. Mattis and J. Bardeen, "Theory of the anomalous skin effect in normal and superconducting metals," *Phys. Rev.*, vol. 111, no. 2, pp. 412–417, 1958.

[19] V. P. Koshelets, S. V. Shitov, A. V. Shchukin, L. V. Filippenko, J. Mygind, and A. V. Ustinov, "Self-pumping effects and radiation linewidth of Josephson flux-flow oscillators," *Phys. Rev. B*, vol. 56, no. 9, 1997, Art. no. 5572.